Characterisation of Ge micro-strip sensors with a micro-focused X-ray beam

M. Borri, C. Cohen, O. Fox, J. Groves, W. Helsby, O. Mathon, L. Mcnicholl, S. Pascarelli, K. Sawhney, R. Torchio, et al.

Nuclear Inst. and Methods in Physics Research, A 988 (2021) 164932

Contents lists available at ScienceDirect

Nuclear Inst. and Methods in Physics Research, A

journal homepage: www.elsevier.com/locate/nima

Characterisation of Ge micro-strip sensors with a micro-focused X-ray beam

M. Borri [a,*], C. Cohen [b], O. Fox [d], J. Groves [a], W. Helsby [a], O. Mathon [b], L. McNicholl [a], S. Pascarelli [b,1], K. Sawhney [d], R. Torchio [b], M. Zuvic [c]

[a] STFC Daresbury Laboratory, Daresbury, Warrington WA4 4AD, United Kingdom
[b] ESRF, 71 Avenue des Martyrs, 38000 Grenoble, France
[c] Mirion Technologies (Canberra), 1 Chemin de la Roseraie, 67380 Lingolsheim, France
[d] Diamond Light Source Ltd., Didcot, Oxfordshire OX11 0, DE, United Kingdom

ARTICLE INFO

Keywords:
Germanium
Micro-strip sensors
Cryogenic detector systems
Hard X-rays
Energy dispersive spectroscopy

ABSTRACT

Germanium micro-strip sensors were selected as the sensor technology to take data in energy dispersive X-ray spectroscopy experiments at the Extremely Brilliant Source (EBS) in Grenoble (FR). It is important for this experimental technique to use sensors with a large uniform area and a fine pitch. The former determines the range of energy detectable with a single sensor. The latter improves spectral resolution. A high stopping power is also important to perform studies with hard X-rays.

The device under test in this measurement was a germanium micro-strip sensor made of 1024 strips with 50 μm pitch. The bulk was 1.5 mm thick. The sensor was assembled into a prototype cryostat part of the XH detector system. The device was tested at the B16 beamline at the Diamond Light Source (DLS) in Didcot (UK). The objective of the test-beam was to characterise charge-sharing between strips. In fact, this effect limits the spectral resolution of the device.

To carry out this test, the sensor was scanned over a subset of strips with micro-focused X-rays under different settings. These were beam energy and intensity, sensor temperature and bias voltage. Results are presented in this paper. It was measured that the full width half maximum of the charge-sharing profile across different strips was ∼90 μm for settings which were indicative of the experimental conditions at the EBS. This was a signal current per unit area on the sensor of $\sim 1.66\times10^{-8}$ A/μm^2, a bias voltage of −180 V and a temperature of −159 °C.

1. Introduction

Germanium micro-strip sensors were selected to take data in energy dispersive X-ray spectroscopy experiments at the Extremely Brilliant Source (EBS) [1] in Grenoble (FR). The EBS is a fourth generation light source providing X-ray beams with high brilliance and coherence. The experimental requirements set by the EBS beams to address new science are met by the development and upgrade of beamline instrumentation like detector systems. In this specific case, the upgrade of a detector system using Ge micro-strip sensors will benefit the High Power Laser Facility (HPLF) [2,3]. This facility will combine a high power laser with the EBS beams to perform dynamic compression experiments. Extreme conditions of pressure and temperature are created in matter. These transient physical states are short-lived (ns) and they are used to study structure and properties of substances in a variety of conditions [4]. These investigations address scientific questions in solid state physics, materials science and energy science.

In its first stage, the HPLF involves installing a 100 J ns-pulse laser (λ = 1053 nm) on the ID24 beamline. This setup performs X-ray Absorption Spectroscopy (XAS) experiments in pump–probe mode. Its distinctive feature is the capability of performing time-resolved Energy Dispersive EXAFS (EDE). EXAFS is the acronym for Extended X-ray Absorption Fine Structure. A second phase in the HPLF project will follow involving a laser upgrade to 200 J and extending the usage to other X-ray techniques such as X-ray diffraction and imaging on an adjacent beamline.

A germanium micro-strip sensor will be used in time-resolved EDE experiments to detect the dispersed spectrum downstream the sample. A sketch of the setup is shown in Fig. 1. The laser pulse acts as a 'pump stimulus' that excites the sample to a short-lived state. An X-ray flash acts as a probe that hits the sample after a predetermined delay with respect to the laser pulse. The X-ray beam exits from the undulators at ID24 and hits a polychromator. It is focused onto the sample and it diverges downstream of it. The micro-strip sensor is

* Corresponding author.
E-mail address: marcello.borri@stfc.ac.uk (M. Borri).
[1] Now at European XFEL - Holzkoppel 4, 22869 Schenefeld, Germany.

https://doi.org/10.1016/j.nima.2020.164932
Received 12 August 2020; Received in revised form 5 November 2020; Accepted 1 December 2020
Available online 3 December 2020

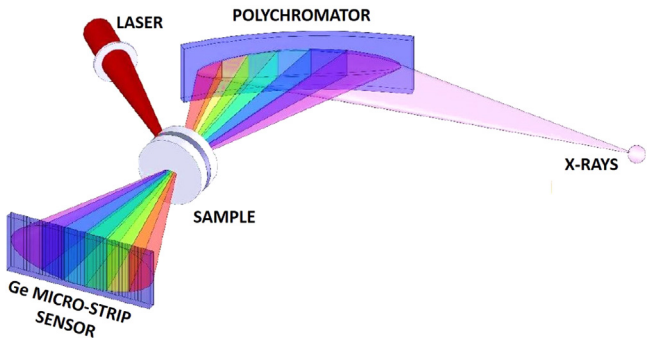

Fig. 1. Sketch of a time-resolved Energy Dispersive EXAFS (EDE) experiment at ID24.

placed behind the sample. Each strip detects the intensity of a specific energy of the transmitted X-rays and the signal is processed by the detector electronics.

The energy resolution of the ID24 energy dispersive spectrometer is set to be comparable to the broadening of the atomic levels caused by the physical process called core-hole life time [5]. The energy resolution on the beamline setup depends on several factors like the X-ray source and the X-ray optics, the focusing distance of the sample (∼1.1 m) and the distance of the detector (∼4 m) from the polychromator. A sensor with a spectral resolution of ∼120 μm is necessary to achieve the accuracy required by the experiments using X-ray beams in range 5–27 keV.

It is expected that the higher photon intensity of a single X-ray pulse at the EBS will reduce photon statistical noise with respect to pre-EBS beams, thereby improving the quality of the measurement.

2. Sensor requirements

It is important for the quality of EDE measurements to select a sensor with a large uniform area and a fine pitch so that good spectra are collected. A large uniform area determines the range of energy detectable with a single sensor. A fine pitch improves spectral resolution.

The stopping power is an important parameter because the sensor needs to fully absorb X-rays in the range of interest. A material with a high stopping power ensures that X-rays are fully absorbed in a relatively thin bulk. The energy range of interest for applications at ID24 is 5–27 keV.

Fast charge collection is important because pump–probe experiments are performed by capturing individual pulses of X-rays. The time given to collect the charge is dictated by the fill pattern of the accelerator. Fast charge collection is determined by a combination of high electric field and a thin bulk. Full charge collection within 700 ns is a fundamental requirement for operations at ID24. At this beamline, the shortest and most challenging configuration requires charge collection within 175 ns.

A fabrication process which is intrinsically resistant to the Total Ionising Dose (TID) is necessary for the longevity of the sensor. The sensor is exposed to the pink beam of the synchrotron integrating TID during its operation. The highest photon flux of 5.6×10^{13} γ/s is expected at a pink beam with central energy of 7 keV during the fill-pattern called 4-bunch mode.

Germanium micro-strip sensors produced by Mirion Technologies [6] were selected as the sensor technology for this application. They provide the best option to fulfil the sensor requirements mentioned above.

The characterization with a micro-focused X-ray beam of one of these sensors is presented in this paper. The goal of this activity is to study charge-sharing between strips. It is important to measure charge-sharing because it determines the spectral resolution and the quality of EDE spectra.

3. Device Under Test (DUT)

The device under test consisted of a germanium micro-strip sensor assembled into a prototype cryostat which is part of the XH system [7,8]. Fig. 2(a) shows a photograph of the cryogenic detector system installed on the B16 Test beamline.

3.1. Sensor

An image of the high-purity germanium micro-strip sensor is shown in Fig. 2(b). The sensor was made of 1024 strips. The strip pitch was 50 μm with a gap of 25 μm and the strip length was 5.0 mm. Two guard-rings surrounded the array of strips. The sensor thickness was 1.5 mm and it is a back illuminated device. Wire bonding pads were placed at the upper-end of odd strips and at the lower-end of even strips. The sensor was manufactured by Mirion Technologies in Lingolsheim (FR) using a proprietary process.

An operational temperature on the sensor ≤−170 °C was defined by measuring leakage current and depletion voltages at different temperatures on test structures. A sensor operated at a temperature ≤−170 °C shows typically values of total leakage current <10 μA at −200 V, and a depletion voltage of ∼−20 V. At higher temperatures, the main effect is an increase of the total leakage current which becomes dominated by the contribution from the guard-rings. In the long term, this effect could shorten the lifetime of the sensor. It was deemed acceptable to test the sensors without damage in the range of temperatures considered in this work.

3.2. Electronics

The electronics were conditioning and reading out the signal from the sensor.

Front-end electronics were housed inside the cryostat. The system used the ASIC called X3CHIP which was designed in AMS 350 nm technology by STFC Rutherford Appleton Laboratory (RAL) in Didcot (UK). The X3CHIP consisted of 128 front-end channels. Each channel had an integrating preamplifier with an adjustable feedback capacitor (2 pF to 40 pF). The output of the preamplifier was sampled at the beginning and at the end of the integration time on a pair of capacitors. The voltage from each of the two capacitors were then multiplexed in parallel onto the analogue outputs. During the read-out cycle, a second pair of capacitors was used to sample the preamplifier output within the integration period. In this way, the read-out and integration periods were overlapped. The settings for the integration time ranged from 180 ns to 1 s. Groups of 32 channels were read-out by a common multiplexer and this equates to a total of 4 multiplexers per ASIC.

The DAQ unit of the system was operated under ambient conditions. It was designed by STFC Daresbury Laboratory in Warrington (UK). In this system, the signals multiplexed from the pre and post integration samples were fed to an instrumentation amplifier forming a correlated double sample, to remove offsets. The signal was in turn digitised by a 14 bit 50 MHz ADC with dynamic range of 1.25 V. A Virtex5 (FX70) FPGA with an embedded microprocessor (400 MHz) read out the data which were then transferred to a PC via 1 Gigabit Ethernet link.

A test-circuit in the ASIC was used to test the entire signal processing chain. A current from the test-circuit was injected at the input of the preamps. A representative measurement of the electrical performance of the system is reported for a feedback capacitor of 10 pF, a fully depleted sensor and an integrated charge of amplitude near the middle of the ADC range. In the case, a signal with an average amplitude of ∼5.3 pC had a standard deviation of ∼1.5 fC. This is equivalent to a signal over noise ratio of ∼3500.

The maximum signal processed by the system was an integrated charge of 50 pC. This was achieved when the 40 pF feedback capacitor was selected in the ASIC preamplifier and its output amplitude reached the top of the dynamic range of the ADC.

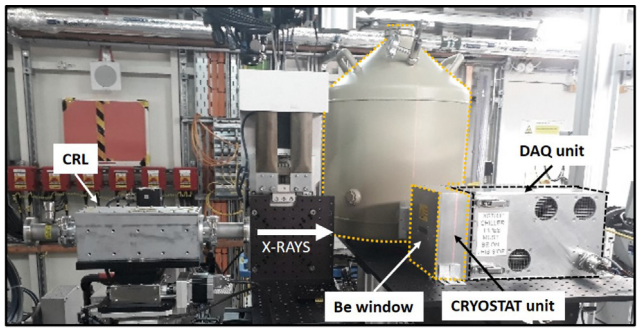

(a)

(b)

Fig. 2. (a) The XH system installed on the B16 beamline at the DLS. The compound refractive lens (CRL) array is placed upstream of the beryllium window of the XH system to micro-focus X-rays onto the sensor. (b) Distinctive features of the germanium micro-strip sensor.

3.3. Mechanics

Sensor and front-end electronics were assembled into a cryostat. A rod connected the liquid nitrogen filled Dewar with a plate supporting the sensor and front-end electronics.

The cryostat used in this project was a prototype. It did not reach a target temperature on the sensor of −170 °C when front-end electronics produced 12 W of power. Nevertheless, it was valid to progress sensor testing while an optimised cryostat was developed.

4. Beamline setup

The measurements presented in this paper were carried out at the B16 Test beamline [9] at the Diamond Light Source (DLS) in Didcot (UK). The beamline uses a water-cooled fixed-exit double-crystal monochromator to deliver monochromatic beams in range 4–20 keV. An unfocused monochromatic beam is provided to the experimental hutch where a compound refractive lens (CRL) array was used to micro-focus the X-rays. The DUT was aligned in Z (i.e. beam direction) at the focal position and positioned on an XY stage to translate the sensor perpendicular to the incident beam. The experimental setup on the B16 beamline is depicted in Fig. 2(a).

The fill pattern of the storage ring during the experiment was single-bunch hybrid mode where a proportion of the fill was made up of a single bunch (3 nC) and the rest was a single contiguous train of bunches (685 bunches of 0.8 nC each, 2 ns apart). The single bunch was separated by a gap of 240 ns from the beginning and the end of the train of bunches.

5. Plan of measurements

The objective of the B16 beamtime was to characterise charge-sharing between strips. This is because this effect limits the spectral resolution in the sensor.

Charge-sharing between strips was investigated by scanning a monochromatic micro-focused beam across the sensor as shown in Fig. 3. The micro-focused beam was incident on the back-side of the sensor. X-rays penetrated the bulk and they were absorbed via photoelectric effect. Produced charge carriers travelled towards the front-side of the sensor where they were collected by strips and then conditioned by front-end electronics. A step size of 2.5 μm was used to move the sensor with respect to the beam in all scans. A total travel path of 502.5 μm was scanned in 201 steps covering an area of ∼10 strips.

Scans with the micro-focused beam were repeated multiple times with settings that explored different operating conditions of beam energy and intensity, sensor temperature and bias voltage. Parameters were combined in nested loops with the beam-energy scan nesting the beam-intensity scan, which was nesting the temperature scan, which was nesting the bias voltage scan. A total of 49 datasets were acquired during the test beamtime.

The size of the beam was measured at the focal plane and in a region of interest along the Z direction for each X-ray energy. This allowed the micro-strip sensor position, inferred from mechanical drawings, to be aligned with the focal plane of the CRL array. As the sensor is enclosed in the cryostat and cannot be seen from outside the Be window, it was estimated that +/-5.0 mm uncertainty on the nominal position was a reasonable assumption.

The beam-energy was set to three different values 10 keV, 15 keV and 20 keV to cover a large sub-range of the operational energy at ID24 (5–27 keV). All three energies do not penetrate further than the first few hundreds of microns as shown in Fig. 4(a). The 15 keV beam has a higher photo-absorption cross-section (91.48 cm^2/g) than the 10.0 keV (37.42 cm^2/g) and the 20.0 keV (42.22 cm^2/g) settings. Consequently, 90% of photons are absorbed within ∼50 μm. X-rays of 10 keV and 20 keV have very similar penetration depths.

The intensity of X-rays was scanned by inserting foils of different thickness and material to absorb the beam. For example, a 1.0 mm Al foil was used to allow transmission of nominally 42% [10] of the original intensity of the 20 keV beam. Scanning the intensity of the instantaneous photon flux affects the density of charge carriers which are generated in the bulk.

The temperature on the sensor was set to three different values −160 °C, −150 °C and −140 °C. The lowest temperature of −160 °C was the best value achievable with the prototype cryostat used in these tests. The temperature affects charge collection processes by impacting the thermal velocity of charge carrier and the trapping processes in the bulk.

Finally, the bias voltage was scanned from −50 V to −180 V in step of 10 V. A high bias voltage produces a higher electric field in the sensor and this influences the drift velocity of charge carriers.

6. Focus scan

The size of the focused beam was measured by moving an Au knife-edge through it and recording the intensity drop on a photo-diode placed behind it. The S-shaped signal from this scan was differentiated and the full width half maximum (FWHM) of this profile was used to estimate the beam size as shown in Fig. 5(a).

The beam size measurement was repeated for several positions along the beam propagation axis (Z) in both the horizontal (X) and vertical (Y) directions with the aim of locating the focal plane and seeing how the beam size varied away from this along Z.

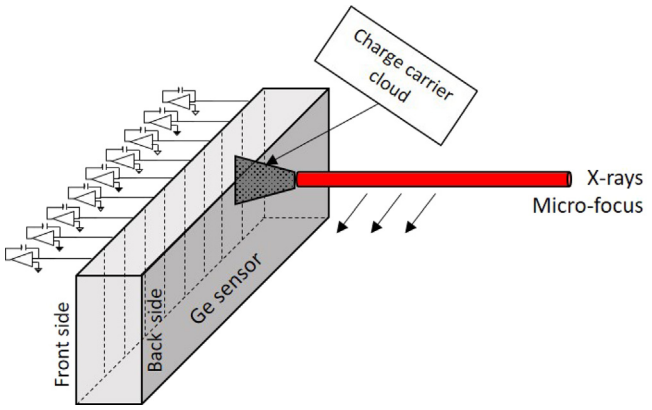

Fig. 3. Sketch of a scan with a micro-focused beam over the sensor.

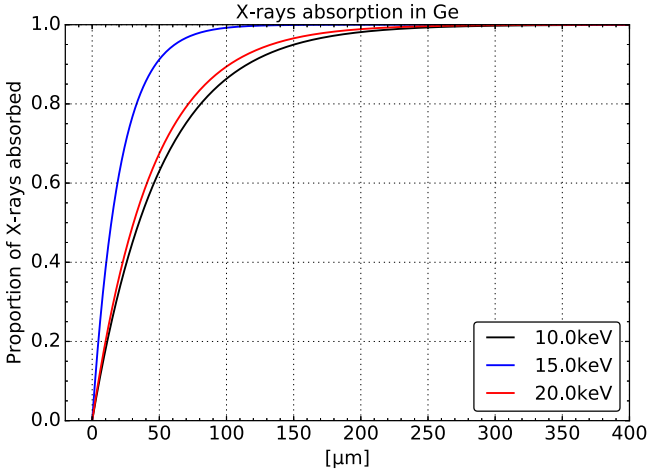

Fig. 4. Photon absorption in germanium at the three beam energies: 10 keV, 15 keV, 20 keV.

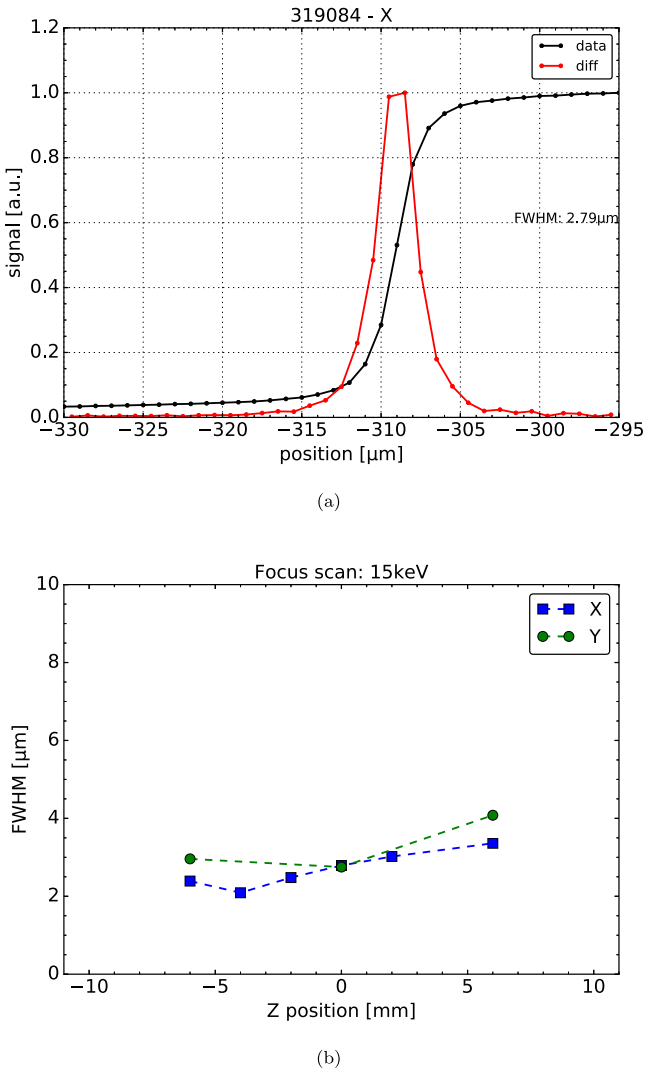

Fig. 5. (a) S-shaped curve of beam intensity signal at 15 keV measured by scanning an Au knife-edge in front of a photodiode (black line). Its derivative (red line) was used to calculate the full width half maximum (FWHM) of the beam spot-size. (b) Focused beam measurement at 15 keV.

The aim was to maintain the spot size as narrow and consistent as possible across the different beam energies. Ideally as close as possible to 5 μm FWHM.

The number of lenses in the CRL array was constant during the experiment so that the focal length required changing for each beam energy. The focal length was ~320 mm at 10 keV, ~700 mm at 15 keV and ~1200 mm at 20 keV. The beam had a narrower depth of focus at 10 keV (Fig. 6(a)) compared to that at the higher energy of 15 keV and 20 keV (Fig. 5(b) and Fig. 6(b), respectively).

A FWHM of the X-ray beam of ~4.0 μm at the focal plane was similar across the different settings.

7. Charge-sharing profile

The charge-sharing profile was the distribution used to compare charge-sharing over different settings and is obtained by recording the signal in a strip as a function of beam position.

Fig. 7 shows the charge-sharing profile in different strips which were within the region of interest scanned by the X-rays (15 keV). The sum of the charge in these strips at each position is also presented and compared to the storage ring current of the synchrotron. As expected, a correlation is observed between the fluctuations in ring current and the total charge.

Fig. 8 shows the charge-sharing profile for a subset of four strips, referred to as channels under test. The charge-sharing profile is compared with the signal distribution in a cluster of a 9 strips centred on the channel under test (i.e. cluster seed). The signal distribution in the cluster of 9 strips refers to the point in the scan where the channel under test recorded its maximum signal. Note that the signal in the cluster of strips has a good overlap with the charge-sharing profile. This is expected and validates the charge-sharing profile as a representation of charge-sharing in the sensor. The FWHM of the charge-sharing profile is employed in the following sections as the parameter to compare charge-sharing at different settings.

8. Charge-sharing for different values of bias voltage

The effect of bias voltage on the charge-sharing profile is presented by plotting the FWHM of the charge-sharing distribution at different bias voltages. The trend is presented for up to three different Regions of Interest (ROIs) at different beam intensities of 1.0 transmission (Fig. 9(a)) and 0.03 transmission (Fig. 9(b)). The sensor temperature and the beam energy were kept constant at −159 °C and 15 keV, respectively.

The response across the regions is uniform for the two different beam intensities. The smallest FWHM is achieved with a low beam intensity and a high bias voltage. The bias voltage has a greater effect on reducing the FWHM at the higher fluxes.

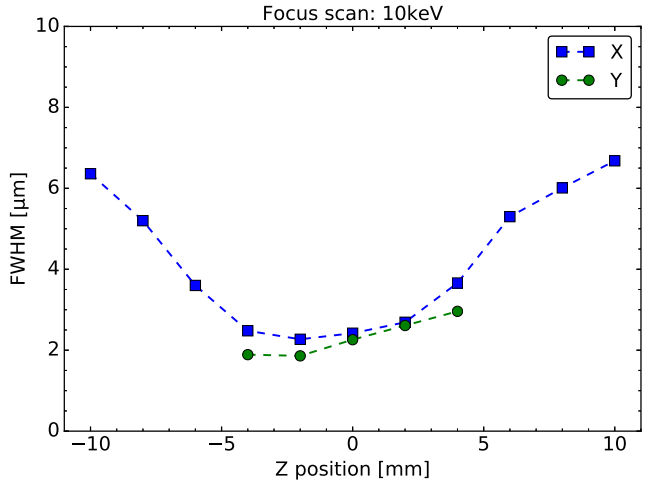

(a)

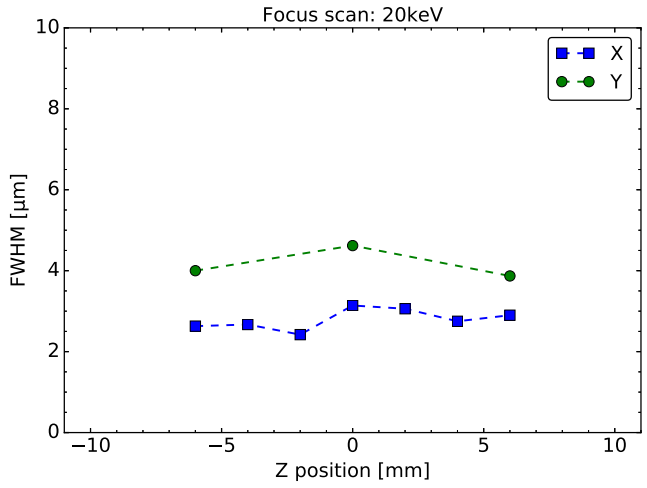

(b)

Fig. 6. Focused beam measurement at 10 keV (a), and at 20 keV (b).

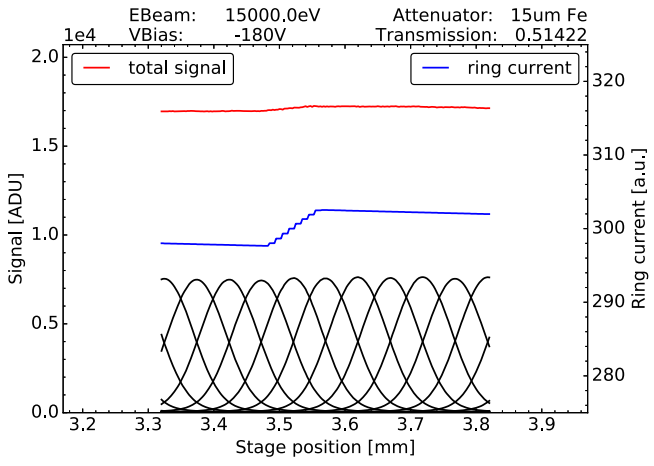

Fig. 7. Signal in analogue-to-digital units (ADU) for different strips within the region of interest recorded as a function of beam position (black lines). As expected, the total signal in the strips (red line) at each beam position follows the variations of the storage ring current (blue line).

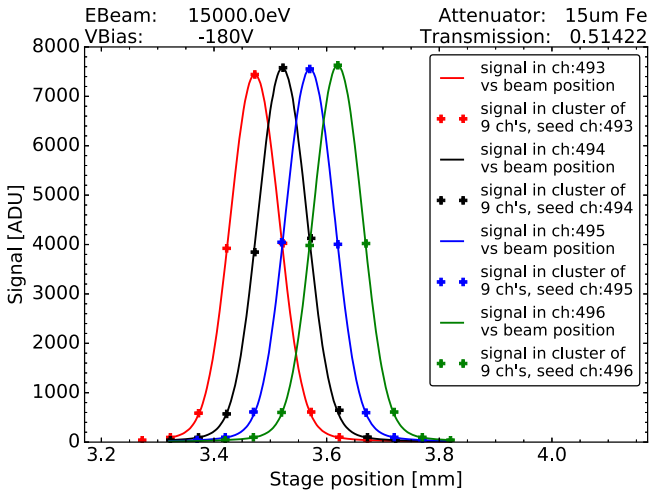

Fig. 8. The signal in ADU is recorded in four selected strips, also called channels under test, as a function of the beam position to obtain the charge-sharing profile (continuous lines). The charge-sharing profile is compared with the signal distribution in a cluster of nine strips (cross markers). The cluster is centred on the channel under test, also called cluster seed, at the point in the scan where it recorded its maximum signal.

9. Charge-sharing for different X-ray energy and intensity

The effect of energy and intensity of X-rays on charge-sharing is investigated in this section. A comparison between datasets is presented by plotting the FWHM of the charge-sharing profile as a function of integrated current. The integrated current can be used as a proxy for the intensity of the X-ray beam across different datasets. In fact, it was necessary to change the integration time of the front-end electronics during data collection in order to compensate the recorded signal for different beam intensities. The shortest integration time was set to 5.0 µs and the longest was set to 500 µs. Therefore, it is not possible to simply compare values of integrated charge. Instead, it is necessary to consider the amount of time over which charge was integrated. Hence, the integrated current was calculated by summing the charge recorded in a cluster of 9 strips around the seed and diving by the integration time. The feedback capacitor (10 pF) was kept constant in all datasets.

A comparison of three beam energies is presented for different bias voltages: −50 V in Fig. 10, −150 V in Fig. 11(a), −180 V in Fig. 11(b). A higher voltage is more effective in containing the spread of the charge-sharing profile created by high intensity beams. The three different beams have comparable charge-sharing profiles at similar beam intensities.

In the following paragraphs the signal current per unit area is used as a proxy to compare test-beam results with operational conditions at ID24. In this beamline, the highest flux is expected at 7 keV during a fill-pattern which is known as 4-bunch mode. In this configuration the bunch length is 107 ps and bunches are separated by 700 ns. A nominal value of 39.6×10^6 γ/bunch with a skewed distribution is delivered to the sensor. This translates to an estimated peak current of 8.30×10^{-5} A on a single strip. The photon flux responsible for this peak current in the strip is delivered over an area of 50 µm×100 µm equal to $\sim 1.66 \times 10^{-8}$ A/µm^2.

During this beamline tests, the spot size on the sensor was considered to be circular with diameter ~4.0 µm. For a current of 5.0×10^{-6} A this leads to a current per unit area of $\sim 4.0 \times 10^{-7}$ A/µm^2. This is an extreme case with respect to the operating conditions at ID24.

For a signal current per unit area of $\sim 1.66 \times 10^{-8}$ A/µm^2 a FWHM of ~90 µm was measured at −180 V. For this bias voltage, the FWHM is <120 µm for all the beam intensities investigated.

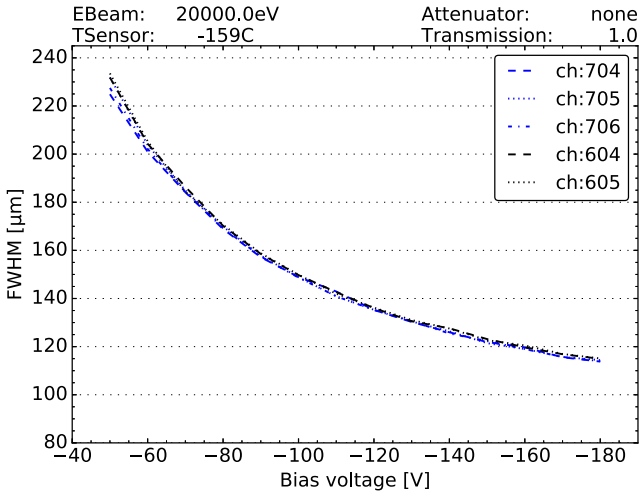

(a)

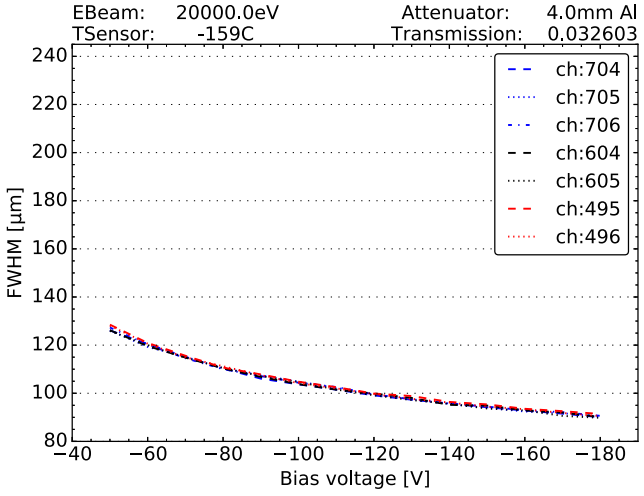

(b)

Fig. 9. (a) FWHM of charge-sharing profile versus bias voltage for 1.0 transmission and five different channels under test. (b) FWHM of charge-sharing profile versus bias voltage for 0.03 transmission and seven different channels under test.

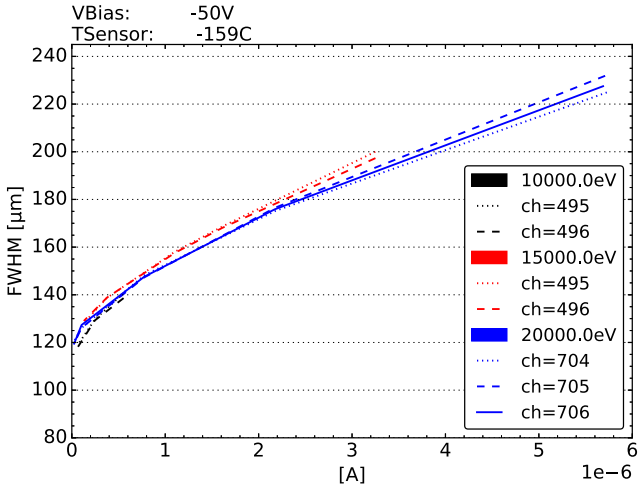

Fig. 10. The FWHM of the charge-sharing profile is plotted as a function of integrated current at a bias voltage of −50V.

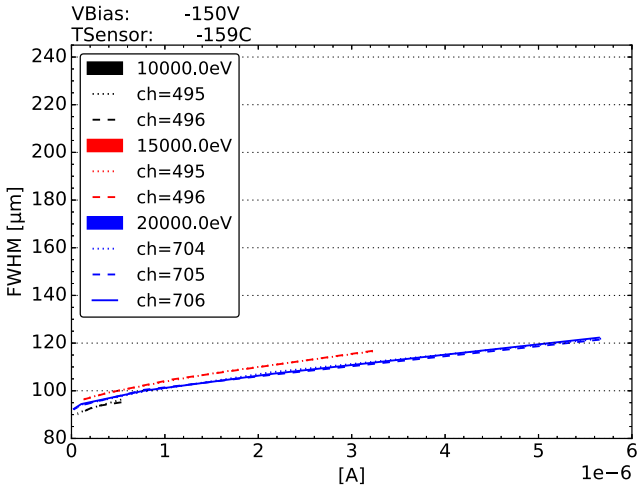

(a)

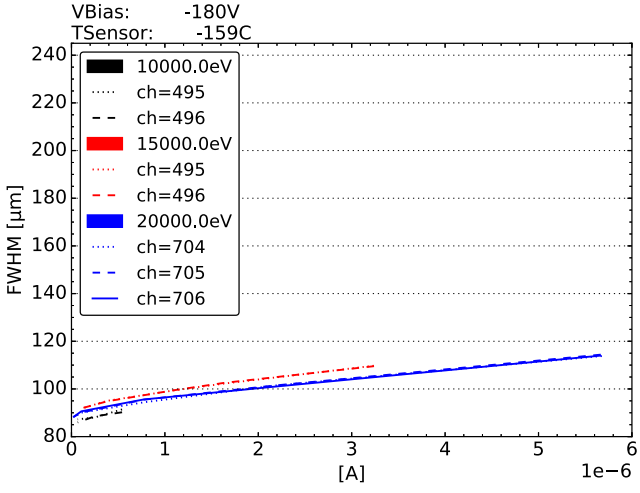

(b)

Fig. 11. The FWHM of the charge-sharing profile is plotted as a function of integrated current. Two different bias voltages are presented: −150 V (a) and −180 V (b).

10. Temperature effects on charge-sharing

Scans of the micro-focused beam across the sensor were repeated under three different temperatures: −159 °C, −150 °C, −140 °C using X-rays of 15 keV. The FWHM of the charge-sharing profile was plotted as a function of bias voltage for a few strips and for each of the three temperatures. The representative case for a beam transmission of 1.0 is shown in Fig. 12(a). It was observed that a warmer sensor leads to a narrower FWHM.

In turn, values of FWHM were compared for a fixed voltage of −180 V in Fig. 12(b). The trend of these curves does not appear linear, although a variation in FHWM of ∼2.0 µm every 10 °C was observed.

11. Conclusion

A high-purity germanium micro-strip sensor was characterised with a micro-focused beam of monochromatic X-rays. The objective of the test was to study charge-sharing between strips because this process limits the sensor spectral resolution in applications of Energy Dispersive EXAFS (EDE). The spot-size of the beam was ∼4.0 µm in all the scans undertaken. Results showed that the dependency of the charge-sharing profile on bias voltage is uniform across different regions of interest.

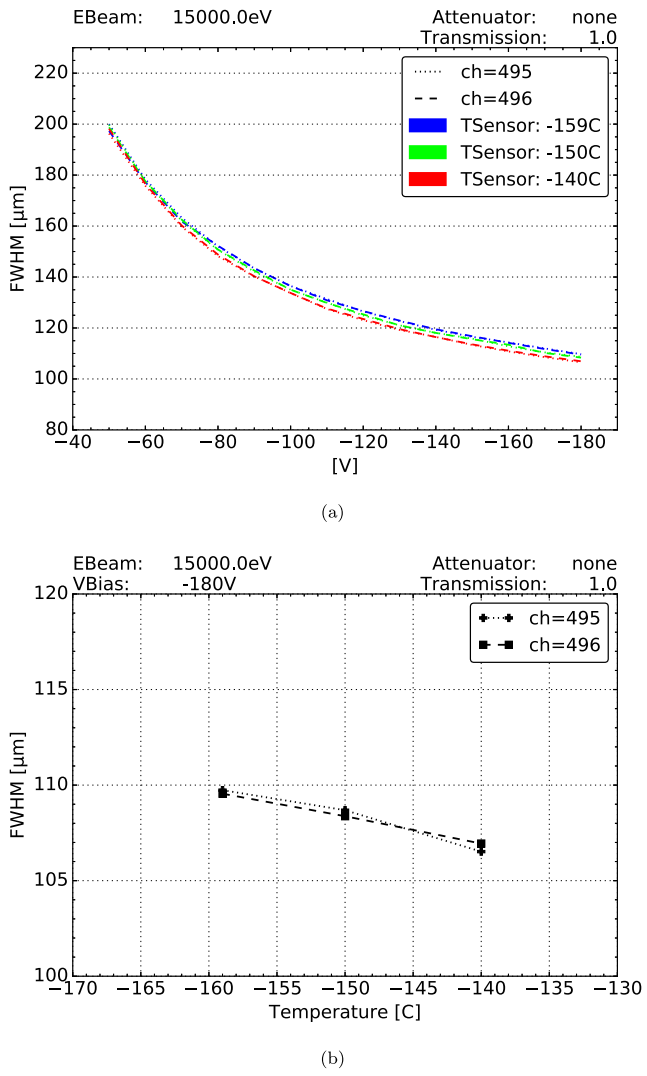

Fig. 12. (a) The FWHM of the charge-sharing profile is plotted as a function of bias voltage for three temperatures and 1.0 transmission. (b) FWHM for a fixed bias voltage (−180 V) as a function of temperature .

The FWHM of the charge-sharing profile across different strips was ∼90 µm for a case indicative of the experimental settings at ID24. Specifically these settings were a signal current per unit area of ∼ 1.66×10^{-8} A/µm^2, a bias voltage of −180 V and sensor temperature of −159 °C. The X-ray intensity worsens the charge-sharing profile even at bias voltages up to −180 V. Beams of three different energies have comparable charge-sharing profiles at similar beam intensities. A higher temperature reduces the FWHM of the charge-sharing distribution by ∼2 µm every 10 °C.

The sensor validation programme is continuing with the aim of installing this sensor technology in a production (optimised) version of the cryostat part of the XH system.

CRediT authorship contribution statement

M. Borri: Formal analysis, Project administration, Funding acquisition, Visualization, Methodology. **C. Cohen:** Investigation. **O. Fox:** Resources. **J. Groves:** Project administration, Funding acquisition. **W. Helsby:** Formal analysis, Funding acquisition, Visualization, Investigation, Methodology. **O. Mathon:** Conceptualization, Funding acquisition. **L. McNicholl:** Investigation. **S. Pascarelli:** Conceptualization, Funding acquisition. **K. Sawhney:** Resources. **R. Torchio:** Conceptualization. **M. Zuvic:** Investigation.

Declaration of competing interest

The authors declare that they have no known competing financial interests or personal relationships that could have appeared to influence the work reported in this paper.

Acknowledgements

The authors would like to acknowledge STFC, United Kingdom for funding this project (RM03-FY19) via the Centre For Instrumentation programme. They would also like to thank the Diamond Light Source for time on beamline B16 under proposal MM24637-1. Finally, they express their gratitude to A.Dent, F.Mosselmans and N.Tartoni at the DLS for helping to organise the test-beam.

References

[1] G. Admans, et al., ESRF Upgrade Programme Phase II (2015-2022) Technical Design Study, 2014, http://www.esrf.eu/Apache_files/Upgrade/ESRF-orange-book.pdf.
[2] S. Pascarelli, et al., The time-resolved and extreme-conditions XAS (TEXAS) facility at the European synchrotron radiation facility: the energy-dispersive X-ray absorption spectroscopy beamline ID24, J. Synchrotron Radiat. 23 (2016) 353–368.
[3] O. Mathon, et al., ESRF high power laser facility project oupling absorption spectroscopy and laser driven shock experiments, in: Talk at Synchrotron Radiation Instrumentation (SRI 2018), 2018, http://sri2018.nsrrc.org.tw/site/userdata/1157/paper/G1.3-0373.pdf.
[4] R. Torchio, et al., Probing local and electronic structure in warm dense matter: single pulse synchrotron x-ray absorption spectroscopy on shocked Fe, Sci. Rep. 6 (2016) 26402.
[5] M. Newille, Fundamentals of XAFS, Rev. Mineral. Geochem. 78 (2014) 33–74.
[6] Mirion Technologies, https://www.mirion.com/.
[7] J. Headspith, et al., First experimental data from XH, a fine pitch germanium microstrip detector for energy dispersive EXAFS (EDE), in: IEEE Nuclear Science Symposium Conference Record, 2007, pp. 2421–2428.
[8] Y. Iwasawa, et al., XAFS Techniques for Catalysts, Nanomaterials, and Surfaces, Springer, 2017, pp. 120–122.
[9] I.P. Dolbnya, et al., A water-cooled monochromator for the B16 test beamline at the diamond light source: capabilities and performance characterization, J. Synchrotron Radiat. 26 (2019) 253–262.
[10] B.L. Henke, et al., X-ray Interactions: photoabsorption, scattering, transmission, and reflection at E=50-30000 eV, Z=1-92, At. Data Nucl. Data Tables 54 (1993) 181–342.